http://dx.doi.org/10.5012/bkcs.2012.33.11.3618

Photodissocaition Dynamics of Propiolic Acid at 212 nm: The OH Production Channel

Myeong Suk Shin, Ji Hye Lee, Hyonseok Hwang, Chan Ho Kwon, and Hong Lae Kim*

*Department of Chemistry, Institute for Molecular Science and Fusion Technology, Kangwon National University, Chunchun 200-701, Korea. *E-mail: hlkim@kangwon.ac.kr*
Received June 27, 2012, Accepted August 7, 2012

Photodissociation dynamics of propiolic acid (HC≡C-COOH) at 212 nm in the gas phase was investigated by measuring rotationally resolved laser-induced fluorescence spectra of OH ($^2\Pi$) radicals exclusively produced in the ground electronic state. From the spectra, internal energies of OH and total translational energy of products were determined. The electronic transition at 212 nm responsible for OH dissociation was assigned as the $\pi_{C\equiv C} \rightarrow \pi^*_{C=O}$ transition by time-dependent density functional theory calculations. Potential energy surfaces of both the ground and electronically excited states were obtained employing quantum chemical calculations. It was suggested that the dissociation of OH from propiolic acid excited at 212 nm should take place along the S_1/T_1 potential energy surfaces after internal conversion and/or intersystem crossing from the initially populated S_2 state based upon the potential energy calculations and model calculations for energy partitioning of the available energy among products.

Key Words : Photodissociation, Propiolic acid, OH, LIF, PES

Introduction

Photophysical and photochemical processes of a molecule upon irradiation of UV light depend on the nature of the excited state and the shape of potential energy surfaces (PES) leading to individual channels.[1] The PES's both on the ground and excited states can be obtained by quantum chemical calculations although it is extremely difficult for the excited states because of complexities due to interactions such as multichannel interferences. Given the PES's, dynamics calculations employing various theories can provide detailed information on the processes of interest. Electronic transitions of the molecule undergoing dissociation usually result in broad, continuous absorption spectra in UV, which can provide little information on the excited states. Photodissociation dynamics, experimentally measured dissociation time and mechanism including model calculations under reasonable assumptions based upon the general shape of the PES thus provides characteristic properties of the molecule on the excited electronic states.

Photodissociation dynamics of saturated carboxylic acids in UV has thoroughly been investigated from which the C-OH bond fission was found to be the major primary dissociation process.[2-8] Quantum yields for the OH production from acetic acid around 220 nm were measured to be around 0.7 by Singlton and coworkers.[2] The dissociation from the initially prepared $^1(n,\pi^*)$ state, the lowest electronic transition in UV, should be correlated to the OH on the ground electronic state whereas the $^1(\pi,\pi^*)$ state should be correlated to both the ground state OH and the CH_3+COOH channel in acetic acid.[4] It was suggested that the OH production from acetic acid should take place along the triplet potential energy surface with a considerable exit channel barrier *via* intersystem crossing manifested by the detailed experimental observations. The unsaturated carboxylic acid such as acrylic acid exhibits similar behavior in photodissociation dynamics in spite of higher conjugation than the saturated carboxylic acids.[9] The C-OH and the C-C bond fissions were found to be the major primary dissociation processes at 193 nm from photofragment velocity distribution measurements. The electronic transition at 193 nm leads acrylic acid to the $^1(\pi,\pi^*)$ state where the structure of the molecule is very different from that on the ground electronic state. From this initially prepared S_2 state, the dissociation of OH occurs along the S_1 or T_2 potential energy surfaces with similar exit channel barriers on both surfaces after internal conversion or intersystem crossing from the S_2 state.

Photodissociation dynamics of another unsaturated carboxylic acid, propiolic acid, was studied at 193 nm by laser induced fluorescence measurement of the OH radicals, from which energy partitioning of the available energy among products was obtained.[10] In addition, fluorescence from the S_1-S_0 radiative transition in the parent molecule was observed. It was concluded that the parent molecule should be excited to the S_2 state at 193 nm and that the dissociation should take place along the S_1/T_1 potential energy surfaces based upon simple quantum chemical molecular orbital calculations compared to the results of acrylic acid. The observed energy distribution was explained by the so-called barrier-impulsive model (or hybrid model). However, the barrier energy and structure of the molecule on top of the barrier required for calculation of the energy distribution upon applying the model were ambiguous because of lack of theoretical calculations. In addition, the UV absorption spectrum would have helped to understand the nature of the excited state and the photodissociation dynamics.

In the present study, the UV absorption spectrum of propiolic acid in the gas phase has been obtained and the

photodissociation dynamics at 212 nm, long wavelength side of the absorption spectrum, has been investigated by measuring rotationally resolved laser-induced fluorescence spectrum of the OH radicals exclusively produced in the ground electronic state. The observed electronic transitions have been identified taking advantage of quantum chemical molecular orbital calculations. In addition, energy partitioning among the fragments has been obtained from the observed spectrum of OH and compared to the model calculations based on the potential energy curves obtained from quantum chemical *ab initio* calculations and the detailed photodissociation dynamics has been discussed.

Experiments

The experiments were carried out in a low pressure flow cell with conventional photolysis-probe geometry. The cell, a cube made of stainless steel with four arms (each 30 cm long) was evacuated to a pressure of 10^{-3} Torr by a mechanical pump. The gaseous sample was slowly flowed through the cell at a pressure of 20 mTorr from a reservoir that contained liquid propiolic acid and the vapor in equilibrium at ambient temperature. The sample pressure was controlled by two needle valves. The liquid propiolic acid (states purity of 98%) was purchased from Aldrich and used without further purification.

The 212 nm, vertically polarized photolysis light (typically 1 mJ/pulse, 4 mm dia.) was generated by mixing after doubling of the fundamental output of a dye laser (Continuum ND-6000) pumped by the second harmonic of an Nd:YAG laser (Continuum Surelite). The probe light to measure the laser-induced fluorescence spectra of OH, employing the $X(^2\Pi) \rightarrow A(^2\Pi)$ electronic transition at 306-320 nm, was a doubled output of another dye laser (Lumonics, HD-500) pumped by the second harmonic of an Nd:YAG laser (Lumonics, YM-800). The two laser beams were collinearly or perpendicularly introduced to the cell through the arms, which contain baffles to minimize scattered radiation. The delay between the photolysis and probe, typically about 100 ns, was controlled with a digital pulse and delay generator. The power of the probe light, which was about 20 μJ/pulse (~4 mm dia.), was kept as low as possible to avoid saturation of the spectra. The fluorescence signal was detected with a photomultiplier tube (Hamammatsu, R-212UH) perpendicularly mounted relative to the two laser beams through cut-off filters and collection lens. The measured signal was fed to a digital sampling oscilloscope and integrated fluorescence signals were recorded. A 20 mTorr sample pressure and 100 ns delay between the photolysis and probe laser pulses ensure measurements of nascent product energy distribution. The fluorescence spectra were corrected with variation of the photolysis and probe laser powers, and the data were collected and stored on a personal computer.

The linewidth of the probe laser output was measured by rotationally resolved gaseous I_2 spectra near 620 nm, which was found to be 0.07 cm^{-1} at FWHM. This laser line profile was deconvoluted from the measured line profiles to estimate the actual Doppler profiles in the spectra.

Results

Electronic Transitions: The UV absorption spectrum of propiolic acid in the gas phase was taken and presented in Figure 1. The spectrum shows continuously increasing absorption starting from around 215 nm with structures near 200 nm. In order to identify the electronic transitions responsible for these peaks, quantum chemical molecular orbital calculations were carried out using the *Gaussian 09* program package.[11] First, the density functional theory (DFT) calculations were performed to obtain the equilibrium structure on the ground state at the B3LYP/6-311++G(p,d) level. The equilibrium geometry on the ground electronic state is planar with hydroxyl proton adopting *cis* or *trans* conformations with respect to the carboxyl group where the *cis* conformer is more stable.[12] Then, vertical excitation energies from the global minimum were calculated by the time dependent-density functional theory (TD-DFT) calculations at the B3LYP/6-311++G(p,d) level (Table 1). The transition responsible for the absorption at 212 nm was found to be mainly the $\pi_{C\equiv C} \rightarrow \pi^*_{C=O}$ transition. In saturated carboxylic acid such as formic acid, the lowest energy transitions in UV are the $n_O \rightarrow \pi^*_{C=O}$ transition that changes the molecular structure

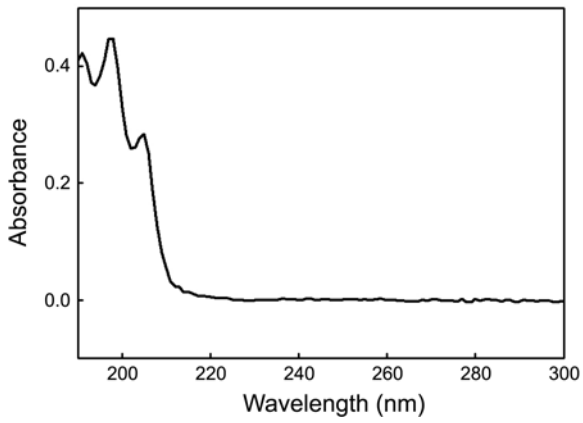

Figure 1. UV absorption spectrum of propiolic acid in the gas phase taken by VARIAN Cary-100 UV-VIS spectrophotometer with the cell path length of 1 cm and the sample pressure of 50 Torr.

Table 1. Results of Molecular Orbital Calculations for propiolic acid

Vertical energy (eV)	Orbital assignment	CI expansion contribution	Oscillator strength
4.76	$\pi_{C=O}$ (18) → $\pi^*_{C=O}$ (19)	0.5079	
5.64	$\pi_{C\equiv C}$ (16) → $\pi^*_{C=O}$ (19)	0.3979	0.0001
5.97	$\pi_{C\equiv C}$ (17) → $\pi^*_{C=O}$ (19)	0.4432	0.0750
6.95	$\pi_{C=O}$ (15) → $\pi^*_{C=O}$ (19)	0.4819	0.0148
6.99	$\pi_{C\equiv C}$ (17) → σ^*_{C-O} (22)	0.6028	0.0003
7.31	$\pi_{C=O}$ (18) → $\pi^*_{C\equiv C}$ (20)	0.7006	0.0250
7.58	$\pi_{C=O}$ (18) → $\pi^*_{C\equiv C}$ (21)	0.7030	0.0394

from planar to pyramidal with the elongated C=O bond resulting in C=O progressions in the absorption spectra.[13,14] In propiolic acid, however, the $\pi_{C\equiv C} \rightarrow \pi^*_{C=O}$ transition does not significantly alter the structure of the parent molecule but only the HCC- moiety lying slightly out of plane. The state associated with $\pi\pi^*_{C=O}$ should be bound with respect to the C-OH bond and dissociation should favor the lower energy channel. The vertical transition takes place at the Franck-Condon region transferring the equilibrium geometry of the ground state to the excited state resulting in the UV spectrum. The parent molecule excited to a place on the excited potential energy surface at the Franck-Condon region that has the $\pi\pi^*_{C=O}$ character experiences surface crossing to the exit channel leading to the dissociation products, which is the C-OH bond breaking channel in the present study. The detailed decay mechanism could be investigated only by the full multi-dimensional potential energy surface including the Franck-Condon and the asymptotic product region.

Energy Partitioning Among Fragments. The enthalpies of formation of propiolic acid and propiolyl radical (HC≡CCO) have never been reported in any literature from experiments and theoretical calculations. Thus, the enthalpy of reaction producing OH from propiolic acid was once estimated from the average values of those of acrylic acid, propenal, and propynal.[15] The enthalpies of formation of propiolic acid and propiolyl radical were calculated in the present study employing the G2(MP2) theory using the *Gaussian 09* program,[16] which are −73.28 and 293.67 kJ/mol, respectively and thus the enthalpy of reaction producing OH to be 409.1 kJ/mol. The enthalpy of reaction was previously obtained by the same calculation within 3% difference from the experimentally measured value in the case of propargyl alcohol.[17] The available energy that is the photon energy at 212 nm (563.9 kJ/mol) minus the enthalpy of reaction was calculated to be 166.7 kJ/mol including 11.9 kJ/mol average thermal energy of the parent molecule, which would be distributed among products.

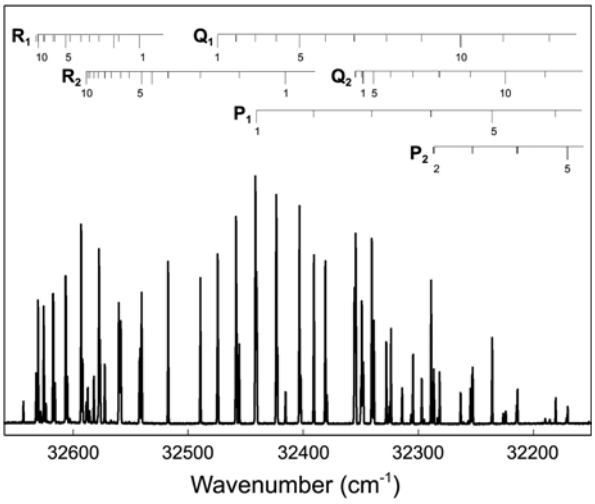

Figure 2. Laser-induced fluorescence spectrum of OH produced from photodissociation of propiolic acid at 212 nm employing the A ← X electronic transition of OH.

The laser-induced fluorescence spectra of OH produced from photodissociation of propiolic acid at 212 nm were measured employing the $X(^2\Pi) \rightarrow A(^2\Pi)$ electronic transition (Figure 2). In the spectra, the 0-0 bandhead of the rovibronic transitions is shown and the well-resolved P-, Q-, and R-branch rotational transitions are observed. The individual rotational transitions are assigned on top of the spectra according to Dieke and Crosswhite.[18] Normalized rotational population distributions were obtained by relative intensities of the observed lines corrected by appropriate line strength factors[19] and Boltzmann-type plots are presented in Figure 3. From the linear regression, the rotational temperature was deduced, from which the average rotational energies of 5.98 ± 0.24 kJ/mol was obtained for v" = 0. The spectra were recorded in the 1-1 band region but no appreciable intensities were measured out of noise and hence negligible population was observed in v" = 1.

The translational energy of the OH fragments was measured from the Doppler broadened rotational lines. In the present experimental set-up, when both the linearly polarized photolysis and probe laser beams are collinearly propagated, the probe direction is perpendicular to the polarization direction of the photolysis laser beam whereas the probe direction is parallel to the polarization direction of the photolysis laser beam when the two laser beams are propagated perpendicular to each other. In both geometries, the observed Doppler profiles of the rotational transitions were Gaussian-like under the resolution of our laser, which implies isotropic velocity distribution of the OH fragments. One might argue that even for the isotropic velocity distribution, the Doppler profiles for different rotational branch transitions should be distinct due to the v-J correlation developed at an instance of dissociation[20] but the shape difference in the profiles could not be resolved in the present study. The Doppler profile of the $P_1(2)$ rotational transition is presented in Figure 4 together with the observed laser line profile. The average translational energy of the OH fragments was calculated from the second moment of the observed profiles after deconvolution of the laser line profile and the center of mass translational energy release in the fragments for the OH rotational state N=2 was then calculated to be 145.3 ± 11.4

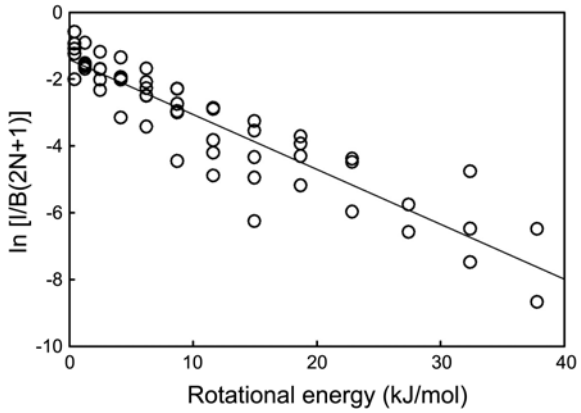

Figure 3. Boltzmann-type plots of rotational population distribution of OH obtained from the spectrum in Figure 2.

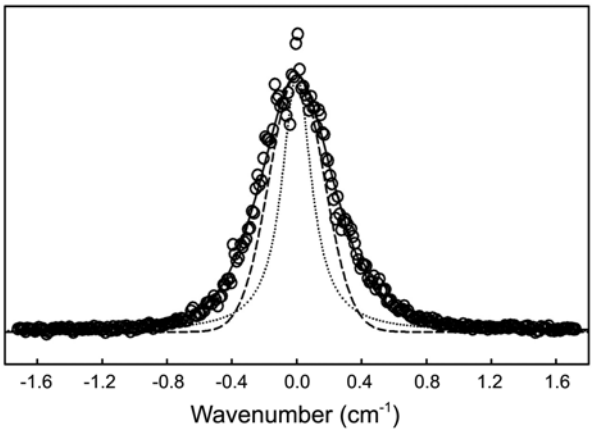

Figure 4. Doppler profile of the $P_1(2)$ rotational transition of OH. The dotted line is the laser line profile. The dashed and the solid lines are the actual Doppler profile and the best fit with convolution of the laser line profile, respectively.

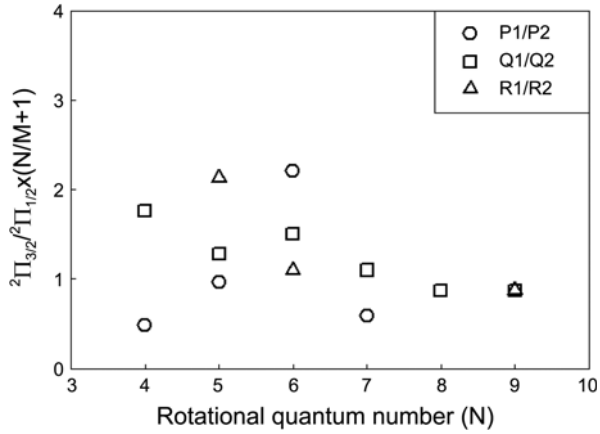

Figure 5. Population ratios between the two spin-orbit states of OH as a function of the rotational quantum numbers.

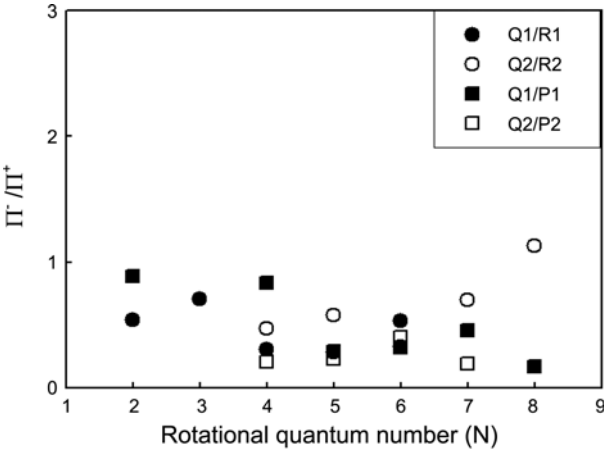

Figure 6. Population ratios between the two Λ-doublet states of OH as a function of the rotational quantum numbers.

kJ/mol. The observed partitioning of the available energy to the products is summarized in Table 2.

F1/F2 and Λ-Doublet Ratios. The observed OH ratio between the two different spin-orbit states, F1($^2\Pi_{3/2}$)/F2 ($^2\Pi_{1/2}$) and between the Λ-doublet states are presented in Figure 5 and 6, respectively. In the present study, the F1/F2 ratio shows no propensity between the two states but slight propensity in one of the Λ-doublet state, the Π+ state was observed. The origin of the propensity in one of the spin-orbit state is not clear but it should be related to the relative time for dissociation to the electron precession and/or singlet-triplet surface interaction.[21] If the dissociation is relatively slow, an electron correlation should somehow determine the final spin-orbit state of the product. However, the Λ-doublet propensity unambiguously originates from the dissociation dynamics.[22,23] If the OH rotation arises from the impulse at the dissociation, the p_π orbital generated from the dissociation should then lie in the plane of rotation resulting in the population of the Π+ Λ-doublet state. The Π- state is populated, however, when the force perpendicular to the plane of rotation such as torsional vibration of OH in the parent molecule is exerted. According to the selection rule, the Q-branch rotational transition should be induced from the Π- state whereas the P- and R-branch transitions should be induced from the Π+ state. Thus, from relative intensities between the different rotational branch transitions, the Λ-doublet population ratio can be measured. In the present study of photodissociation of propiolic acid, a slight propensity in the Π+ Λ-doublet state was observed implying that the OH rotation should mainly originate rather from the impulse at an instant of dissociation than the force acting perpendicular to the plane of rotation such as torsion. As

Table 2. Energy partitioning (in kJ/mol) among products with fractions of the available energy from photodissociation of propiolic acid at 212 nm for the OH v" = 0 state

	Available energy	$<E_r(OH)>$	$<f_r(OH)>$	$<E_t(sys)>$	$<f_t>$
212 nm	166.7				
	Experiment	5.98 ± 0.24	0.036	145.3 ± 11.4	0.87
	Prior	9.66	0.058	33.07	0.20
	Impulsive	6.81	0.040	151.9	0.91
	BIM[a]	23.4	0.14	64.50	0.39
193 nm[b]	178.6				
	Experiment	6.28	0.035	134.7	0.75
	BIM	7.53	0.042	134.7	0.75

[a]Barrier Impulsive Model with reverse barrier of 39.7 kJ/mol. [b]ref. 10, BIM with the reverse barrier of 156.9 kJ/mol.

mentioned above, in this case, a positive v-J correlation should be developed resulting in unique Doppler profiles in the spectra for the Q and P, R-branch rotational transitions, respectively but the small differences between the shape of the profiles could not be distinguished under our resolution in the present study.

Discussion

All of the models proposed to explain mechanisms of photodissociation followed by an electronic transition range between the statistical model at one end and the impulsive model at the other end. The impulsive model can be applied to direct, fast dissociation from repulsive excited states, whereas the statistical model is applied to slow dissociation from the vibrationally hot ground electronic state after rapid internal conversion. In each case, the dissociation dynamics is vastly different and thus, the resulting physical properties of the product systems are different. In the case of indirect dissociation due to extensive potential couplings between the excited states, however, the physical properties of the final products such as energy partitioning among products cannot be expected by simple models, because the dissociation dynamics should be governed by the shape of the potential energy surface leading to the individual product channels.

In order to figure out the shape of the potential energy surface for the OH dissociation channel, first, the potential energies of the parent molecule on the ground electronic state was calculated as a function of the C-O bond distance by the DFT calculations (Figure 7). The energy of the molecule at equilibrium was first calculated and then, optimized structures and energies were obtained as the C-O bond distance was extended by 0.1 Å step up to 3.5 Å where the molecule is assumed to be dissociated at this distance. These calculations were performed at the B3LYP/6-311++G(p,d) level using the *Gaussian 09* program package.[11] The OH dissociation energy from these calculations was found to be 405.0 kJ/mol compared with 409.1 kJ/mol mentioned above. Similar results were obtained by *ab initio* calculations at the MP2/6-311++G(d,p) level, which is not shown in the figure. For the potential energy surface on the excited electronic state, the optimized structures and energies of the molecule on the S_1 and S_2 states were first obtained by the time-dependent DFT (TD-DFT) calculations with the 6-311++G (d,p) basis. The adiabatic transition energies for the S_1 and S_2 states from the bottom of the potential energy curve on the ground electronic state are 386.3 and 484.7 kJ/mol, respectively. Then, the same TD-DFT calculations were performed for the molecule with the C-O bond extending up to the dissociation limit, 3.5 Å with geometry optimization. The similar potential energy surfaces for the excited states leading to the OH production channel were once calculated at the CIS and the TD-DFT level but those calculations provided the single point energies with the frozen geometries as the equilibrium geometry on the ground electronic state.[24] As a result, the calculated potential energies were not along

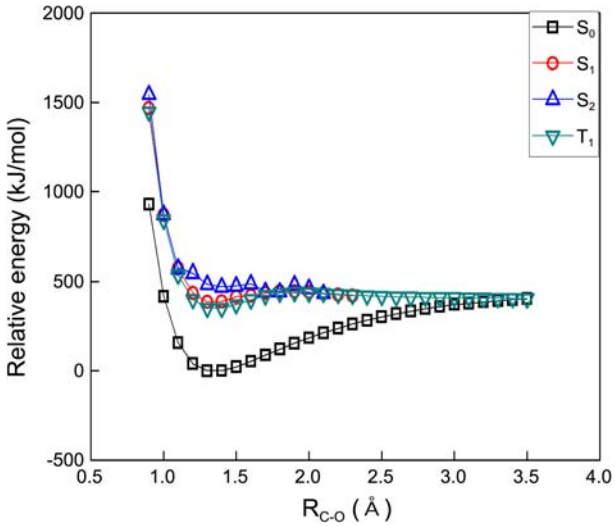

Figure 7. Potential energy curves in the ground, T_1, S_1, and S_2 excited states leading to the OH production channel in propiolic acid. Squares and reverse triangles are the energies on the ground state and the T_1 state obtained by the DFT calculations, respectively. Circles and triangles are the energies on the S_1 and the S_2 states obtained by the TD-DFT calculations, respectively.

the reaction coordinate but along an artificially chosen coordinate such as a ridge on the surface because it was not the minimum energy path. The adiabatic potential energy curves as a function of the C-O bond distance, the reaction coordinate, are shown in Figure 7. The curves show slightly bound nature along the C-O dissociation coordinate with small exit channel barriers, which would originate from differences in molecular structures between the ground and excited electronic states and/or the potential curve crossings between the excited states. The T_1 excited state is also the molecular state that can be correlated to the product state, that is, the two doublet spin states. The DFT calculations were also performed for the optimized energy and the structure on the T_1 state and the adiabatic potential energy curve along the dissociation coordinate, the C-O distance, was obtained under the B3LYP/6-311++G(d, p) level. The T_1 excited state also appears slightly bound with a small exit channel barrier.

The initial $\pi_{C\equiv C} \rightarrow \pi^*_{C=O}$ transition at 212 nm delivers the parent molecule to the Franck-Condon region coupled to the S_2 state that is energetically accessible. The molecule after fast non-radiative relaxation to the bottom of the S_2 state may fluorescence to the S_1 and subsequently to the S_0 state or directly to the S_0 state. The fluorescence observed near 300 nm ($\tau \sim 300$ ns) at 193 nm excitation would be due to this S_1 to S_0 radiative relaxation.[10] The parent molecule on the S_2 state would dissociate along the S_1/T_1 potential energy surfaces after fast internal conversion and/or intersystem crossing, which is a competing process with the radiative transition.

The statistical model can be applied to obtain the energy partitioning among products when the dissociation is slow on the vibrationally hot ground electronic surface after the internal conversion. A simple prior model in this case assumes

that the available energy should be distributed among all product degrees of freedom with equal probability.[25,26] Thus, the population of the individual rotational state of OH is proportional to the number of accessible quantum states in the propiolyl fragment at the energy, $E = E_{av} - E_{OH}(v, J)$. The number of vibrational states of the propiolyl radical was directly counted with fundamental frequencies obtained by the similar DFT calculations at the B3LYP/6-311++G(p,d) level. The calculated average rotational energy of OH from the rotational population distribution is 9.66 kJ/mol. In addition, the average translational energy was also calculated employing the same prior model to be 33.07 kJ/mol, which is very different from the measured values. Therefore, the dissociation should take place on the excited potential energy surface.

When the dissociation occurs on the electronically excited state, the dissociation dynamics should be governed by the shape of the potential energy surface leading to the products. In the case of dissociation where there exists an energy barrier at the exit channel along the reaction coordinate, the barrier-impulsive model can be applied to estimate the energy partitioning among the products.[27] The barrier-impulsive model has long been applied to calculate energy partitioning among products for various unimolecular decomposition reactions with an exit channel barrier such as molecular elimination of HX (X = F, Cl) from haloalkanes.[28,29] In this model, it is assumed that the available energy above the barrier is statistically partitioned among products and the rest is partitioned impulsively from the top of the barrier. On the ground state, the unimolecular decomposition of simple bond rupture producing two radical products has no reverse barrier for association in general but on the excited state, the association reaction of two radicals sometimes has a barrier because of a structural difference between the ground and excited states. Although the barrier-impulsive model has mostly been applied to the reactions on the ground electronic state, it would be applied to the reaction on the excited electronic state when the barrier at the exit channel exits.[30] In this case, it is assumed that the parent molecule spends some time, such as a few vibrational periods, at the Franck-Condon region and is dissociated impulsively on top of the barrier. Thus, the amount of energy of the reverse barrier, E^{imp} would be partitioned impulsively and the rest of the available energy, $E^{stat} = E_{av} - E^{imp}$ is statistically partitioned among the products. The statistical energy partitioning among products for E^{stat} of the available energy was calculated employing the prior model. Using this model and the obtained E^{imp} from the potential energy surface calculations, the rotational energy of OH and the center of mass translational energy release including the energy statistically partitioned was calculated to be 23.44 and 47.70 kJ/mol, respectively, which are again significantly different from the measured values. The measured and calculated energies of the fragments are listed in Table 2. In the table, the energy partitioning from photodissociation at 193 nm is also presented from the literature,[10] from which the barrier impulsive model seems in good agreement with the experiment but the reverse barrier in the previous study was estimated to be very large from the potential energy surface calculations due to reasons mentioned above.

The energy partitioning of the available energy among products can be estimated by the impulsive model when the dissociation of OH from propiolic acid takes place fast from the repulsive part of the S_1 surface,[31,32] In this model, an abrupt turn-on of repulsive force between atoms of the breaking bond is assumed, which results in large translational energy release to the products. Invoking linear and angular momentum conservations, the average translational and rotational energies of the OH fragments were calculated employing the equilibrium geometry calculated from the DFT calculations mentioned above according to the Franck-Condon principle. The calculated center of mass translational energy released to the products and average rotational energy of OH are 151.9 and 6.81 kJ/mol, respectively, which are in good agreement with the experimentally measured values. The effect of reverse barrier is insignificant during the course of dissociation because of little difference in molecular structures on both the ground and the S_1 state. Although the shape of PES is similar to S_1, a propensity of one of the spin-orbit states in OH would be observed if the dissociation takes place on the T_1 surface after intersystem crossing from S_1. In addition, conservation of planar molecular symmetry would prevent the electronic state from crossing to another state. However, the possibility of dissociation along the T_1 surface should still not be excluded.

Conclusions

The photodissociation dynamics of propiolic acid at 212 nm in the gas phase was investigated by measuring the rotationally resolved laser-induced fluorescence spectra of OH produced in the ground state. The electronic absorption at 212 nm leading to dissociation of OH is assigned to the $\pi_{C\equiv C} \rightarrow \pi^*_{C=O}$ transition, from which the dissociation takes place on the S_1/T_1 excited state potential energy surface after internal conversion or intersystem crossing. The ground, S_1, T_1, and S_2 excited state potential energy curves along the dissociation coordinate were obtained by the DFT and TD-DFT calculations. The dissociation takes place on the repulsive part of the S_1 potential energy surface and the observed energy partitioning was successfully modeled by the impulsive model.

Acknowledgments. This work was financially supported by the National Research Foundation (2011-0015288).

References

1. Schinke, R. *Photodissociation Dynamics*; Cambridge University Press: Cambridge, 1993.
2. Singleton, D. L.; Paraskevopoulos, G.; Irwin, R. S. *J. Phys. Chem.* **1990**, *94*, 695.
3. Hunnicutt, S. S.; Waits, L. D.; Guest, J. A. *J. Phys. Chem.* **1989**, *93*, 5188.
4. Hunnicutt, S. S.; Waits, L. D.; Guest, J. A. *J. Phys. Chem.* **1991**,

95, 562.
5. Peterman, D. R.; Daniel, R. G.; Horwits, R. J.; Guest, J. A. *Chem. Phys. Lett*. **1995**, *236*, 564.
6. North, S. W.; Blank, D. A.; Gezelter, J. D.; Longfellow, C. A.; Lee, Y. T. *J. Chem. Phys*. **1995**, *102*, 4447.
7. Owrunski, J. C.; Baronavski, A. P. *J. Chem. Phys*. **1999**, *111*, 7329.
8. Kwon, H. T.; Shin, S. K.; Kim, S. K.; Kim, H. L. *J. Phys. Chem. A* **2001**, *105*, 6775.
9. Kitchen, D. C.; Forde, N. R.; Butler, L. J. *J. Phys. Chem. A* **1997**, *101*, 6603.
10. Kumar, A.; Upadhyaya, H. P.; Naik, P. D.; Maity, D. K.; Mittal, J. P. *J. Phys. Chem. A* **2002**, *49*, 11847.
11. *Gaussian 09*: Gaussian Inc.: Pittsburgh, PA, 2009.
12. Van, C. A.; Schaefer, L.; Siam, K.; Ewbank, J. D. *J. Mol. Struct*. (*Theochem*) **1989**, *56*, 271.
13. Ng, T. L.; Bell, S. *J. Mol. Spectros*. **1974**, *50*, 166.
14. Demoulin, D. *Chem. Phys*. **1976**, *17*, 471.
15. Benson, S. W. *Thermochemical Kinetics*; John Wiley and Sons: New York, 1968.
16. Curtiss, L. A.; Raghavachari, K.; Redfern, P. C.; Pople, J. A. *J. Chem. Phys.* **1997**, *106*, 1063.
17. Lee, J. H.; Hwang, H.; Kwon, C. H.; Kim, H. L. *J. Phys. Chem. A* **2010**, *114*, 2053.
18. Dieke, G. H.; Crosswhite, H. M. *J. Quant. Spectrosc. Radiat. Transfer* **1962**, *2*, 97.
19. Chidsey, I. L.; Crosley, D. R. *J. Quant. Spectrosc. Radiat. Transfer* **1980**, *23*, 187.
20. North, S. W.; Hall, G. E. *J. Chem. Phys*. **1996**, *104*, 1864.
21. Lee, K. W.; Lee, K. S.; Jung, K. H.; Volpp, H. R. *J. Chem. Phys*. **2002**, *117*, 9266.
22. Andresen, P.; Rothe, E. W. *J. Chem. Phys*. **1985**, *82*, 3634.
23. Hanazaki, I. *Chem. Phys. Lett*. **1993**, *201*, 301.
24. Kumar, A.; Naik, P. D. *Chem. Phys. Lett*. **2006**, *422*, 152.
25. Levin, R. D.; Bernstein, R. B. *Molecular Reaction Dynamics and Chemical Reactivity*; Oxford Univ. Press: New York, 1987.
26. Zamir, E.; Levin, R. D. *Chem. Phys*. **1980**, *52*, 253.
27. Robinson, P. J.; Holbrook, K. A. *Unimolecular Reactions*; Wiley: New York, 1972.
28. Arunan, E.; Wategaonkar, S. J.; Setser, D. W. *J. Phys. Chem*. **1991**, *95*, 1539.
29. Dong, E.; Setser, D. W.; Hase, W. L.; Song, K. *J. Phys. Chem. A* **2006**, *110*, 1484.
30. Chang, A. H. H.; Hwang, D. W.; Yang, X. M.; Mebel, A. M.; Lin, S. H.; Lee, Y. T. *J. Chem. Phys*. **1999**, *110*, 10810.
31. Busch, G. E.; Wilson, K. R. *J. Chem. Phys*. **1972**, *56*, 3626.
32. Tuck, A. F. *J. Chem. Soc. Faraday Trans. II* **1977**, *73*, 689.